IN-34
19365

NASA Technical Memorandum 104439
ICOMP-91-10; AIAA-91-1916

Navier-Stokes Simulation of the Supersonic Combustion Flowfield in a Ram Accelerator

8 p

Shaye Yungster
Institute for Computational Mechanics in Propulsion
Lewis Research Center
Cleveland, Ohio

Prepared for the
27th Joint Propulsion Conference
cosponsored by the AIAA, SAE, ASME, and ASEE
Sacramento, California, June 24-27, 1991

NASA

INSTITUTE FOR COMPUTATIONAL MECHANICS IN PROPULSION
NASA LEWIS RESEARCH CENTER
ICOMP
CASE WESTERN RESERVE UNIVERSITY

Navier-Stokes Simulation of the Supersonic Combustion Flowfield in a Ram Accelerator

Shaye Yungster*
Institute for Computational Mechanics in Propulsion
NASA Lewis Research Center, Cleveland, OH 44135

Abstract

A computational study of the ram accelerator, a ramjet-in-tube device for accelerating projectiles to ultra-high velocities, is presented. The analysis is carried out using a fully implicit TVD scheme that efficiently solves the Reynolds-averaged Navier-Stokes equations and the species continuity equations associated with a finite rate combustion model. Previous analyses of this concept have been based on inviscid assumptions. The present results indicate that viscous effects are of primary importance; in all the cases studied, shock-induced combustion always started in the boundary layer. The effects of Mach number, mixture composition, pressure, and turbulence are investigated for various configurations. Two types of combustion processes, one stable and the other unstable, have been observed depending on the inflow conditions. In the unstable case, a detonation wave is formed, which propagates upstream and unstarts the ram accelerator. In the stable case, a solution that converges to steady-state is obtained, in which the combustion wave remains stationary with respect to the ram accelerator projectile. The possibility of stabilizing the detonation wave by means of a backward facing step is also investigated. In addition to these studies, two numerical techniques have been tested. These two techniques are vector extrapolation to accelerate convergence, and a diagonal formulation that eliminates the expense of inverting large block matrices that arise in chemically reacting flows.

Introduction

The ram accelerator is a ramjet-in-tube concept in which a shaped projectile can in principle be accelerated efficiently to velocities in excess of 10 km/s by means of detonation waves or other shock-induced combustion modes. This concept, developed at the University of Washington[1,2], can be scaled for projectile masses ranging from grams to hundreds of kilograms, and has the potential for a number of applications, such as hypervelocity impact physics, direct launch to orbit of acceleration insensitive payloads, and hypersonic testing[3,4]. In the last application, the ram accelerator can be used as a hypersonic research facility for studying hypersonic aerodynamics and the supersonic combustion flowfields of interest to the National Aerospace Plane (NASP) program. An experimental ram accelerator device, currently operating at the University of Washington[5,6], has reached velocities in excess of 2.5 km/sec and Mach numbers as high as 8.4.

Although several ram accelerator operation modes have been proposed[1], the analysis in this paper will be centered on the "superdetonative" mode shown in Fig. 1. In order to operate in this combustion mode, the projectile must fly at superdetonative speeds, i.e., speeds above the Chapman-Jouguet detonation speed of the gas mixture. The gasdynamic principles that govern the flow and combustion processes in the superdetonative ram accelerator are similar to those related to hypersonic airbreathing propulsion systems, particularly to the oblique detonation wave engine[7] (ODWE). However, the device is operated in a different manner.

In the superdetonative ram accelerator (Fig. 1), the centerbody is a projectile fired into a tube filled with a premixed gaseous fuel/oxidizer mixture. There is no propellant on board the projectile. Ignition of the fuel/oxidizer mixture is achieved by means of a series of shock waves that increase its temperature. When the ignition temperature is reached at a designed location, rapid chemical reactions release energy into the flowing stream. The energy addition will establish either a detonation wave or a shock-deflagration wave, depending primarily on the mixture composition, pressure and tube size. The combustion process creates a high pressure region over the back of the projectile, producing a thrust force. The pressure, composition, chemical energy density

*Research Associate. Member AIAA

and speed of sound of the mixture can be controlled to optimize the performance for a given flight condition. Since the fuel and oxidizer in the ram accelerator concept are premixed, the difficulties in obtaining rapid and complete mixing encountered by the ODWE (and the conventional scramjet) are circumvented.

The performance of the superdetonative ram accelerator has been evaluated in the past by using one of the following two approaches: 1) simplified one-dimensional flow models, and 2) numerical simulations based on computational fluid dynamics (CFD) methods.

Simplified one-dimensional models have been developed by Rom & Kivity[8] and Humphrey[9]. Their analysis is based on the jump conditions across the leading oblique shock and across the reflected (and assumed planar) detonation wave. It is further assumed that the flow aft of the detonation is in a state of chemical equilibrium. Yip et. al.[10] included the effects of nonequilibrium chemistry by using a streamtube analysis close to the surface of the projectile. Their approach, however, decouples the chemistry and the fluid dynamics and therefore does not take proper account of the effects of heat release on the shock wave structure.

The main disadvantage of the above models is that they can be applied only to analyze the "nominal" operating condition. The ram accelerator is said to be operating at the nominal condition when the reflected shock wave from the tube wall intersects the shoulder (corner) of the projectile. The expansion wave exactly cancels the reflected shock and no shock or expansion waves are transmitted downstream. For a given flight condition, optimum performance will be achieved by operating at the nominal design condition. Ram accelerator operation at the nominal condition, however, will occur only at the start of the projectile flight. As the projectile accelerates, the angle between the leading conical shock and the projectile will decrease, and the reflected shock (detonation) wave will impinge on the projectile at a location aft of the shoulder, giving rise to a multiple shock-expansion pattern. In addition, reaching this nominal operating condition is difficult in practice, since at high Mach numbers the angle between the leading shock and the projectile is very small (about 3° at $M = 8$), and therefore the clearance between the projectile and the tube wall will have to be very small. The calculations of Humphrey[9] show that at a speed of 4 km/sec, for example, the projectile diameter will have to be 92.4% of the tube diameter (compared to 76% for a typical experimental setup) in order to attain the nominal operation condition. For the tube diameter of 38 mm considered, this implies that the clearance between projectile and tube will be less than 1.5 mm, which is smaller than the boundary layer thickness predicted in the present study at similar conditions.

Analysis of the superdetonative ram accelerator concept based on inviscid computational fluid dynamic methods have been conducted by Bogdanoff & Brackett[11,12] and Yungster, et. al[13,14]. The CFD studies of Bogdanoff and Brackett were based on first and second order Godunov type differencing procedures. A global Arrhenius rate equation was used to model the combustion process, with the Arrhenius constants determined from experimental ignition delay studies. The results presented by Yungster, et. al., were obtained using the point implicit, total variation diminishing (TVD) MacCormack scheme. The analysis used a 7-species, 8-step reaction mechanism for hydrogen-oxygen combustion.

The results presented in all the above studies have confirmed the potential of the ram accelerator to efficiently accelerate large masses (up to hundreds of kilograms) to velocities in excess of 10 km/sec. In these studies, however, the effects of viscosity, heat conduction and mass diffusion have all been neglected. This has been a necessary first step in determining the performance capabilities of the ram accelerator. However, recent studies conducted by the author on shock-wave/boundary layer interactions in premixed combustible gases[15], indicate that viscous effects can be important. In the present paper, numerical simulations of the superdetonative ram accelerator are obtained using the full Reynolds-averaged Navier-Stokes equations and a finite-rate combustion model. The effects of Mach number, mixture composition, pressure, and turbulence are investigated for various configurations. The numerical formulation used is discussed below, preceding the presentation of the computational results.

Numerical Formulation

A complete description of the numerical scheme used in this study has been previously presented in Ref. 15; therefore, it will only be discussed in general terms here.

The Reynolds-averaged Navier-Stokes equations coupled with chemical nonequilibrium processes are considered. The equations are written in nondimensional variables and in generalized coordinates. The thermodynamic transport properties, such as the specific heat, thermal conductivity and viscosity for each species are determined by fourth-order polynomials of temperature. The thermal conductivity and viscosity of the mixture are calculated using Wilke's mixing rule. The binary mass diffusivity between any two species is obtained using the Chapman-Enskog theory in conjunction with the Lennard-Jones intermolecular potential functions.

In the present study, a 7-species, 8-step reaction mechanism for hydrogen-oxygen combustion is adopted. This model is a reduced reaction mechanism obtained from more complete models by the exclusion of the reactions involving H_2O_2 and HO_2, (which could be important in low temperature ignition studies). A complete description of the reduced model and a discussion of its accuracy

and range of application can be found in Refs. 13-15. A more complete 9-species, 18-step combustion model has been recently implemented for testing several variations of the basic iterative scheme used in the present work (to be discussed below).

The turbulent model adopted in the present study is the Baldwin-Lomax algebraic eddy viscosity model[25] and assumes constant turbulent Prandtl and Schmidt numbers ($Pr_t = Sc_t = 0.9$). This model is chosen for its simplicity and computational efficiency.

The interactions between turbulence and chemistry, which enter into the numerical formulation through the source term w_i, represent a very difficult problem. To account for such interaction effects would require a closure method such as the probability density function (PDF) approach or a direct numerical simulation (DNS). Since effective PDF closure methods are not yet available and DNS methods are currently applicable only to relatively simple flows, the interactions between turbulence and chemistry are not considered in the present study.

The fully coupled Navier-Stokes equations and species continuity equations are solved using a new fully implicit finite difference CFD code. The code employs an iterative method that is based on the lower-upper symmetric successive overrelaxation (LU-SSOR) implicit factorization scheme, and a second order symmetric total variation diminishing (TVD) differencing scheme. To accelerate the convergence of the basic iterative procedure, this code can be combined with vector extrapolation methods, such as the Minimal Polynomial (MPE) and the Reduced Rank (RRE) Extrapolation. The extrapolation procedure solves a linear least squares problem and produces a sequence of approximations that, in general, has better convergence properties than the sequence obtained from the iterative scheme alone. A detailed description of these extrapolation techniques can be found in Refs. 16 and 17.

Two different formulations of the LU-SSOR factorization scheme are currently implemented. In one formulation, the implicit operator includes the full Jacobian matrix of the chemical source term, leading to a preconditioner matrix of size $n_s \times n_s$, where n_s is the number of species; this matrix has to be inverted at every grid point. If the number of species considered is large, inverting this preconditioner can be very expensive. Therefore, a second formulation has been introduced. In this technique, the Jacobian matrix is replaced by a diagonal matrix that is designed to approximate the time scaling effects obtained by using the full Jacobian. No matrix inversions are required in this formulation. Several diagonalization methods were tested. The diagonalization method of Imlay, et. al[18] gave the best results. However, this method was found to be less efficient than the full Jacobian formulation. The details of the diagonalization method can be found in Refs. 18 and 19.

Computational test of the numerical techniques

Figure 2 shows the density residual history obtained with the two formulations (full Jacobian and Imlay's diagonalization) with and without extrapolation, for the case of a supersonic flow of a stoichiometric H_2-air mixture past a compression corner. The chemical nonequilibrium processes are simulated by using a 9-species, 18-step finite-rate combustion model. When extrapolation is used, it is started after N_0 iterations, and is implemented in the so called "cycling" mode, using a sequence of K_{max} vectors obtained from the iterative scheme. The overhead in CPU time due to the use of extrapolation is very small (less than 1%) in the present case. The results indicate that savings of up to 40% in the overall computational work required to reach convergence can be realized by using RRE in combination with the basic iterative scheme (using both formulations). Similar results are obtained with MPE. The results also indicate that for the present chemistry model, the diagonal formulation is less efficient, requiring approximately 45% more CPU time than the Full Jacobian formulation to reach convergence.

Results

When analizing shock-induced combustion phenomena, it is sometimes necessary to distinguish between a detonation wave and a shock-deflagration wave. In the literature, different definitions have been used in the past for different problems. In the present study, the following terminology will be used:

1) A shock-deflagration wave is defined as a shock-induced combustion process in which the interaction between shock and combustion is weak; the chemical reactions do not affect significantly the shock. In this process, the shock and the combustion front are essentially decoupled.

2) A detonation wave is defined, following Pratt[20], as a shock-induced combustion process in which "the combustion front follows so closely on the igniting shock wave that the two waves are fully pressure-coupled".

Strictly speaking, the second definition applies to a coupled shock-deflagration wave, since a "true" self-sustaining detonation wave has, in addition to being fully pressure-coupled, a characteristic nonsteady three-dimensional cell structure. Also, the first definition is sometimes applied to a decoupled shock-deflagration wave.

In the present study, no distinction will be made between a detonation wave (as defined above) and a self-sustaining detonation wave. Computations carried out on blunt projectiles fired into detonable gases have shown that the present numerical formulation can successfully reproduce the various shock-induced combustion regimes

observed in these flows. These regimes include decoupled and coupled shock-deflagration waves, and combinations of self-sustaining oblique and overdriven detonation waves[13].

Turbulent Flow Calculations

The computational studies of the superdetonative ram accelerator concept are carried out for configurations having dimensions similar to those of the experimental device presently operating at the University of Washington[1,5,6]. The first set of computations were conducted for the following geometry and inflow conditions:

Referring to Fig. 1, the projectile half angle cone is set to $\theta = 14°$, the tube diameter is $d_t = 3.0$ cm, the maximum projectile diameter is $d_p = 1.95$ cm, and its length is $L = 15$ cm. The flow is assumed to be fully turbulent along the entire projectile. A constant projectile surface temperature $T_w = 600°$K is also assumed. The gas mixture is stoichiometric H_2-air at a fill pressure of $p_\infty = 1$ atm, and a temperature of $T_\infty = 300°$K.

Figure 3 shows the converged solutions obtained on a 157×45 grid at three different Mach numbers. Nondimensional temperature contour lines (T/T_∞) are plotted on the top half of the projectile, and nondimensional pressure color contours (p/p_∞) are plotted on the bottom half. For clarity, all contour plots of ram accelerator configurations are magnified in the vertical direction by a factor of 2. In Fig. 3a, the combustion process starts in the boundary layer at a location immediately behind the point where the reflected shock wave from the tube wall impinges on the projectile. The combustion that begins in the boundary layer propagates outwards and downstream, and a shock-deflagration wave is established.

For a higher Mach number flow ($M = 7.5$), combustion begins prematurely in the boundary layer at the nose region of the projectile, as shown in Fig. 3b. A very complex interaction between the shock-wave system and the chemically reacting boundary layer is observed. Complete combustion is achieved behind the shock being reflected from the projectile surface. At a still higher Mach number, $M = 8$, combustion takes place along the entire boundary layer in the nose region of the projectile, as shown in Fig. 3c. Complete combustion is achieved in this case behind the first reflected shock wave from the tube wall. Note that in all of the three cases above, a high pressure region over the back of the projectile is created, and as a result, a positive thrust force is produced in all three cases.

The pressure distribution along the projectile surface and tube wall for all three Mach numbers is shown in Fig. 4. Note again the higher pressures over the tail of the projectile as compared to the nose. For the $M = 6.7$ and $M = 7.5$ cases the pressure increases in two stages, corresponding to the two shocks impinging on the projectile. Also note the small pressure disturbance created by the reacting boundary layer at the nose for the $M = 7.5$ case. The maximum pressures are obtained on the tube wall for all three cases. The peak pressure observed for the $M = 8$ case has a value around forty times the fill pressure.

Figure 5 shows the variation of y^+ at points nearest the wall, the skin friction coefficient, $c_f = \tau/\frac{1}{2}\rho_\infty U_\infty^2$, and the heat transfer coefficient, $c_h = k\frac{\partial T}{\partial n}/\frac{1}{2}\rho_\infty U_\infty^3$. The value of the Reynolds number $Re = \rho_\infty U_\infty L/\mu_\infty$ for the $M = 6.7$, 7.5 and 8.0 was $1.81 \times 10^7, 2.03 \times 10^7$ and 2.16×10^7, respectively. Ideally, one should have $y^+ = O(1)$ everywhere; this is the case for most of the constant diameter section of the ram accelerator. However, the boundary layer resolution is not good enough at the nose and tail sections resulting in too high y^+ values. Attempts to improve the resolution in these sections of the projectile resulted in computational cells with a very high aspect ratio ($\delta x/\delta y > 1000$) in the constant area part of the projectile; this considerably slowed down or even prevented convergence.

The skin friction coefficient plot, in Fig 5b, shows that combustion causes a reduction in the skin friction and creates a high-temperature, low-density boundary layer that is more susceptible to separation than a similar nonreacting case. A separation bubble is observed for the $M = 6.7$ case near the rear shoulder; a larger one occurs for the $M = 8$ case near the front shoulder. The heat transfer coefficient, shown in Fig. 5c, tends to follow the same qualitative variations as the pressure, decreasing across an expansion wave and increasing across a shock wave.

Figure 6 shows the Mach number profile for the $M = 6.7$ case at the $x/L = 0.35$ station which corresponds to the beginning of the constant diameter section of the projectile. This figure indicates that, for fully turbulent flow, the boundary layer thickness is approximately $\delta/L \approx 0.012$, or $\delta \approx 1.8$ mm. This fairly thick boundary layer suggest that operating the ram accelerator at nominal conditions may not be possible since the clearance between the projectile and the tube will have to be smaller than δ. Further more, the boundary layer grows as the square of the Mach number, making the clearance problem even more severe as the projectile accelerates.

A nondimensional pressure thrust, $\bar{F}$, can be defined as:

$$\bar{F} = \frac{F}{p_\infty A_t} \tag{1}$$

where F is the pressure thrust, p_∞ is the fill pressure, and A_t is the tube area. The pressure thrust F is calculated by numerically integrating the pressure over the projectile surface.

The nondimensional skin friction drag is similarly calculated by integrating the skin friction over the projectile

surface. The net thrust generated in the ram accelerator is calculated by subtracting the skin friction drag from the pressure thrust. Table 1 summarizes the results obtained with this configuration. It is important to point out that even for the cases where premature combustion occurs in the boundary layer at the frontal part of the projectile, a net positive thrust is still obtained.

Also listed in Table 1 is the thrust pressure ratio, ϕ_t, defined as the net average drive pressure on the projectile (the net thrust divided by the maximum projectile cross-sectional area) divided by the maximum cycle pressure. This parameter provides a measure of the device's launch capability versus the maximum pressure the projectile and launch tube must withstand.

The next calculation was conducted with a slightly different configuration, having $d_t = 3.8$ cm, and $d_p = 2.5$ cm, and using a mixture of $2H_2 + O_2 + 5Ar$. The addition of a diluent, such as Argon, to the combustible mixture is typically done in order to change its speed of sound. By doing this, a different velocity range can be covered with the same projectile.

In order to compare the results with those obtained in the previous case (at $M = 6.7$), the conditions were selected so that the maximum temperature in the boundary layer for nonreacting flow is about the same as in the previous $M = 6.7$ case (about 1200°K). Thus, the ignition process will occur at similar temperatures. The same peak temperature as the H_2-air mixture was obtained for $T_w = 300$°K, and $M = 5.8$. The Reynolds number was 1.72×10^7 in this case. For this mixture, the shock waves are stronger at a given Mach number than those obtained for the H_2-air mixture due to a higher value of $\gamma_\infty = (c_p/c_v)_\infty$ (1.53 vs. 1.40). Starting from a nonreacting solution, the result of this calculation is shown in Fig 7 in the form of nondimensional temperature contours (top half) and Mach number contours (bottom half). The results are shown at various iteration stages starting from the nonreacting solution†. A completely different behavior is obtained in this case. The combustion process begins in the boundary layer (Fig. 7a), with no apparent separation. The combustion process seems to establish a detonation wave (Fig. 7b). Note the much steeper angle of this detonation wave compared to the shock-deflagration wave in Fig 3a. The detonation wave produces a separation of the boundary layer (Fig. 7c). The separation bubble continues to grow larger as the detonation wave moves upstream (Figs. 7d and 7e), until what appears to be an overdriven detonation wave is formed (Fig. 7f). At this point, a large pressure will be produced over the frontal part of the projectile resulting in a net drag force. This phenomena is caused entirely by viscous interactions, since no such behavior was previously observed in inviscid calculations[13,14].

† The numerical method used in the present study is first or second order accurate in time for nonreacting flows. For chemically reacting flows, however, the equations become stiff and the numerical scheme solves the stiffness problem by preconditioning the equations, essentially rescaling them in time such that all chemical and convective phenomena evolve on comparable pseudo-time scales. Therefore, the results shown in Fig. 7 are not strictly time accurate, but rather they show the evolution of the iteration process on a pseudo-time scale.

Laminar Flow Calculations

To determine the extent of the turbulence model effect on the flow and combustion processes in the ram accelerator, a series of calculations were performed assuming laminar flow. The geometry used in this case is $d_t = 3.6$ cm and $d_p = 2.52$ cm, and only the frontal part of the projectile was considered ($0 \leq x/L \leq 0.61$). Figure 8 shows the converged solution for a $M = 6.5$ flow in a stoichiometric H_2-air mixture at $p_\infty = 1$ atm, and $T_w = 600$°K. The results show that a separation bubble is formed by the shock wave/boundary layer interaction, and that the combustion process remains confined to the boundary layer. Most of the combustion occurs downstream of the shock, but some combustion is seen to propagate upstream into the separation bubble.

Next, p_∞ is increased to 10 atm. The results for this case are shown in Fig. 9. Under these conditions, combustion upstream of the shock is enhanced by the higher pressure (Fig. 9b), and the temperature inside the separation bubble is much higher than for the $p_\infty = 1$ atm case. The enhanced combustion enlarges the separation bubble and generates a secondary shock ahead of it. This shock wave is strong enough to ignite the main flow, and the shock/combustion wave moves upstream.

The laminar flow results for a $2H_2 + O_2 + 5Ar$ mixture at $p_\infty = 1$ atm and $M = 6.5$ are shown in Fig. 10. As for the turbulent case, the combustion process that starts in the boundary layer (Fig. 10a) evolves into a detonation wave (Fig. 10b). The combustion then propagates upstream through the boundary layer expanding the separation bubble (Figs. 10c-10e) and generating additional shocks as in the case of the H_2-air mixture (Fig. 9).

Thus, it seems that the unstable combustion mechanism is caused by a sequence of boundary layer separation, upstream propagation of the combustion process through the boundary layer, and generation of secondary shock/detonation waves. The process appears to be enhanced by turbulence and by increasing the fill pressure.

Laminar Flow Calculations with a Backward Facing Step

A numerical study was conducted on a projectile having a backward facing step, with the purpose of testing if such a configuration could stabilize the combustion process, by serving as a barrier preventing the upstream propagation

of combustion. For this purpose, a two-block modification of the CFD code was developed and tested first on a simple parallel supersonic flow over a backward facing step. The calculations were compared with experimental results obtained by Donaldson[21] for a $M = 3.5$ laminar flow past a 1.9 cm backward facing step. The Reynolds number based on the length ahead of the step is 1.2×10^6. The computational results are presented in Fig. 11 in the form of pressure contours and velocity vectors. The pressure contour plot (Fig. 11a) shows the leading edge shock wave created by the boundary layer growth, the expansion wave at the corner of the step, and the reattachment shock. The main and secondary recirculation regions behind the step are illustrated in the velocity vector plot shown in Fig. 11b.

Experimental data consisted of the wall pressure distribution and profiles of static pressure at three locations downstream of the step. Figure 12a presents the comparison of the wall pressure distribution behind the step. The pressure is normalized by the inflow static pressure. Figure 12b shows comparisons of the normalized static pressure profile at three locations downstream of the step: $x/h = 0.0537, 2.137$, and 4.279. These comparisons indicate good agreement between the CFD and experimental results, which verify that the multi-block code can predict accurately laminar supersonic flowfields over a step.

Following this benchmark test case, the code was applied to a ram accelerator configuration including a backward facing step, the schematic of which is shown in Fig. 13. A 91×45 and 83×77 grid is used for the two blocks, respectively. The height of the step is 11% of the maximum projectile radius, the Mach number of the incident flow is 4.8, the wall temperature is taken as 600°K and the flow is assumed to be laminar. Figure 14 shows the nondimensional temperature contours and velocity vector field behind the step for the nonreacting solution. The reflected shock wave from the tube wall strongly affects the flow in the recirculation area. Compared with the results shown in Fig. 11, it is observed that the flow now circulates in the opposite direction. The shock wave creates a strong pressure gradient and modifies the circulation pattern. The reacting flow solution is shown in Fig. 15. Reactions start again in the boundary layer behind the shock impingement point. The combustion is then seen to propagate into the recirculation zone. The combustion process expands the recirculation zone and generates a secondary shock, which is strong enough to ignite the main flow above the recirculating zone and a detonation wave is established. The detonation wave then continues to propagate upstream. Increasing the height of the step could perhaps produce better results, but it will also considerably diminish the performance of the ram accelerator. Therefore, alternative configurations should be investigated as a continuation of this work.

Conclusions

A CFD code developed for solving the fully coupled two-dimensional/axisymmetric Reynolds-averaged Navier-Stokes equations including finite rate chemistry has been used for studying the flow, combustion and performance characteristics of the superdetonative ram accelerator concept. Vector extrapolation methods used in combination with the basic iterative scheme show potential for significant savings in the overall computational work. A diagonalized formulation was tested for the combustion of a premixed H_2-air supersonic flow over a compression corner, and was found to be less efficient than the original full Jacobian formulation.

The results obtained for the ram accelerator configuration indicate that viscous effects are of primary importance. Combustion always started in the boundary layer, and two types of combustion processes, one stable and the other unstable, were established depending on the inflow conditions. In the unstable case, a detonation wave is formed, which propagates upstream and unstarts the ram accelerator. In the stable case, a solution that converges to steady-state is obtained, in which the combustion wave remains stationary with respect to the ram accelerator projectile. The unstable combustion mechanism appears to be caused by a sequence of boundary layer separation, upstream propagation of the combustion process through the boundary layer, and generation of secondary shock/detonation waves. The process appears to be enhanced by turbulence and by increasing the fill pressure. The performance characteristics of a stable ram accelerator configuration were computed at various Mach numbers. The results indicate that a positive net thrust can be obtained even when combustion occurs in the nose boundary layer. The possibility of stabilizing the detonation wave by means of a backward facing step was also investigated. This approach appears to be impractical for the configuration studied. A more systematic investigation of shock wave/boundary layer interactions in premixed combustible gases, and of alternative ram accelerator configurations, should be carried out as a continuation of this work.

Acknowledgments

The author would like to acknowledge the support provided by the Numerical Aerodynamic Simulation Program (NAS).

References

1. Hertzberg, A., Bruckner, A.P. and Bogdanoff, D.W., "Ram Accelerator : A New Chemical Method for Accelerating Projectiles to Ultrahigh Velocities," *AIAA Journal*, vol. 26, Feb. 1988, pp 195-203.

2. Bruckner, A.P., Knowlen, C., Hertzberg, A. and Bogdanoff, D.W., "Operational Characteristics of the Thermally Choked Ram Accelerator," to be published in *Journal of Propulsion and Power.*

3. Bruckner, A.P. and Hertzberg, A., "Ram Accelerator Direct Launch System for Space Cargo," Paper No. IAF-87-211, 38th Congress of the International Astronautical Federation, Brighton, England, Oct. 1987.

4. Kaloupis, P. and Bruckner, A.P., "The Ram Accelerator: A Chemically Driven Mass Launcher," AIAA Paper 88-2968, July 1988.

5. Hertzberg, A., Bruckner, A.P. and Knowlen,C., "Experimental Investigation of Ram Accelerator Propulsion Modes," *Shock Wave International Journal*, vol. 1, No. 1, Jan. 1991.

6. Kull, A., Burnham, E., Knowlen, C., Hertzberg, A. and Bruckner, A.P., "Experimental Studies of Superdetonative Ram Accelerator Modes," AIAA Paper 89-2632, July 1989.

7. Morrison, R.B., "Oblique Detonation Wave Ramjet Report," Universal Systems Inc., Contract NAS1-14771, January 1978.

8. Rom, J. and Kivity, Y., "Accelerating Projectiles up to 12 km/s Utilizing the Continuous Detonation Propulsion Method," AIAA Paper 88-2969, July 1988.

9. Humphrey, J.W., "Parametric Study of an ODW Scramaccelerator for Hypersonic Test Facilities," AIAA Paper 90-2470, July 1990.

10. Yip, G.T., Strawa, A.W. and Chapman, G.T., "Streamtube Analysis of Supersonic Combustion in an In-Tube-Scramjet," AIAA Paper 90-2339, July 1990.

11. Brackett, D.C. and Bogdanoff, D.W., "Computational Investigation of Oblique Detonation Ramjet-in-Tube Concepts," *Journal of Propulsion and Power,* vol. 5, No. 3, May-June 1989, pp. 276-281.

12. Bogdanoff, D.W. and Brackett, D.C., "A Computational Fluid Dynamics Code for the Investigation of Ramjet-in-Tube Concepts," AIAA Paper 87-1978, June 1987.

13. Yungster, S., Eberhardt, S. and Bruckner, A.P., "Numerical Simulation of Hypervelocity Projectiles in Detonable Gases," *AIAA Journal*, vol. 29, No. 2, Feb. 1991, pp 187-199.

14. Yungster, S. and Bruckner, A.P., "A Numerical Study of the Ram Accelerator Concept in the Superdetonative Velocity Range," AIAA Paper 89-2677, July 1989. (To be published in *Journal of Propulsion and Power*).

15. Yungster, S., "Numerical Study of Shock Wave Boundary Layer Interactions in Premixed Hydrogen-Air Hypersonic Flows," NASA TM-103273 (also ICOMP-90-22; AIAA paper 91-0413), Jan. 1991.

16. Sidi, A. and Celestina, M.L., "Convergence Acceleration for Vector Sequences and Applications to Computational Fluid Dynamics," NASA TM-101327, ICOMP-88-17, Aug. 1988.

17. Sidi, A., "Efficient Implementation of Minimal Polynomial and Reduced Rank Extrapolation Methods," NASA TM-103240, ICOMP-90-20, Aug. 1990.

18. Imlay, S.T., Roberts, D.W., Soetrisno, M. and Eberhardt, S., "Nonequilibrium Thermo-Chemical Calculations Using a Diagonal Implicit Scheme," AIAA Paper 91-0468, Jan. 1991.

19. Eberhardt, S. and Imlay, S., "A Diagonal Implicit Scheme for Computing Flows with Finite-Rate Chemistry," AIAA Paper 90-1577, June 1990.

20. Pratt, D.T., Humphrey, J.W. and Glenn, D.E., "Morphology of Standing Oblique Detonation Waves," AIAA Paper 87-1785, June 1987.

21. Donaldson, J.C., "An Experimental Study of the Region of Separated Flow Downstream of a 0.75 in. Rearward Facing Step at Mach Numbers 2.5, 3.5 and 5.0," AECE TR 69-141, July 1969.

Table 1: Performance characteristics of the ram accelerator

	Mach number M	Pressure thrust $\tilde{F}$	Skin friction drag $\tilde{D}$	Net thrust $\tilde{F}_{net}$	Thrust pressure ratio ϕ_t
1	6.7	3.60	0.55	3.05	17.68
2	7.5	2.43	0.53	1.90	12.41
3	8.0	2.09	0.45	1.64	8.21

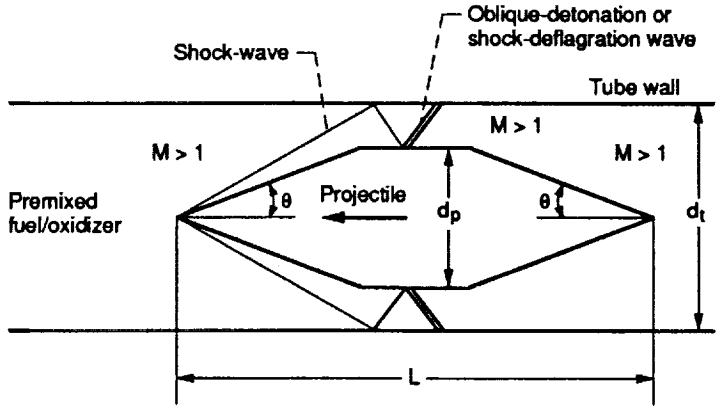

Figure. 1 Schematic of superdetonative ram accelerator mode.

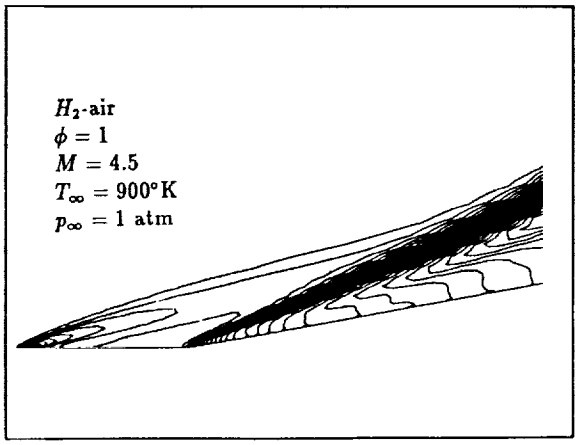

a) Pressure contours

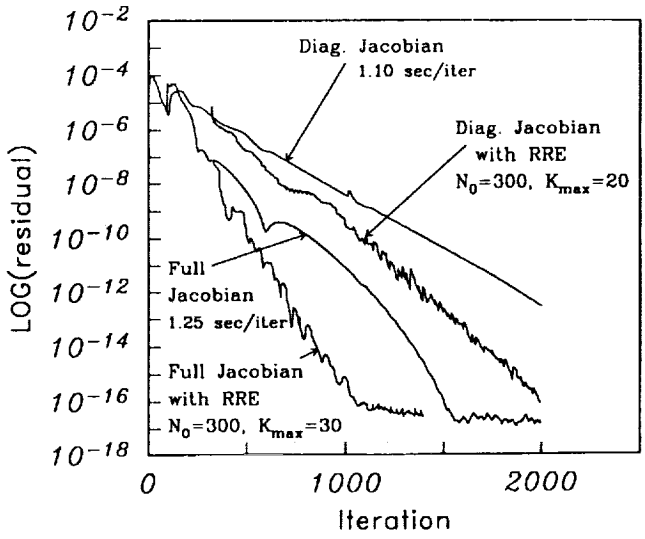

(b) Convergence history of L_2 density residual

Figure. 2 Supersonic reacting flow past a compression corner, (grid: 80 × 50).

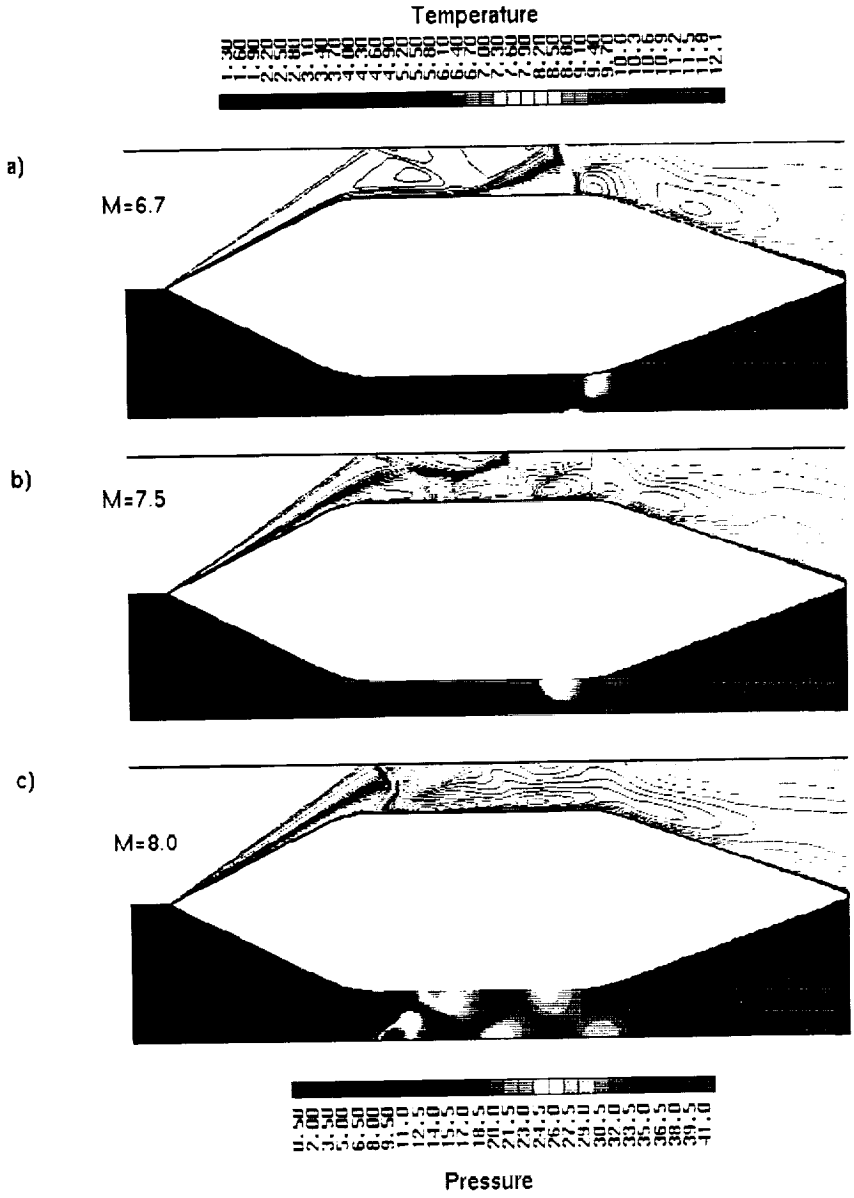

Figure. 3 Nondimensional temperature T/T_∞ (top half), and pressure p/p_∞ (bottom half) contours showing converged solution for reacting turbulent flow (for clarity, the vertical direction is magnified by a factor of 2). Mixture: stoichiometric H_2-air.

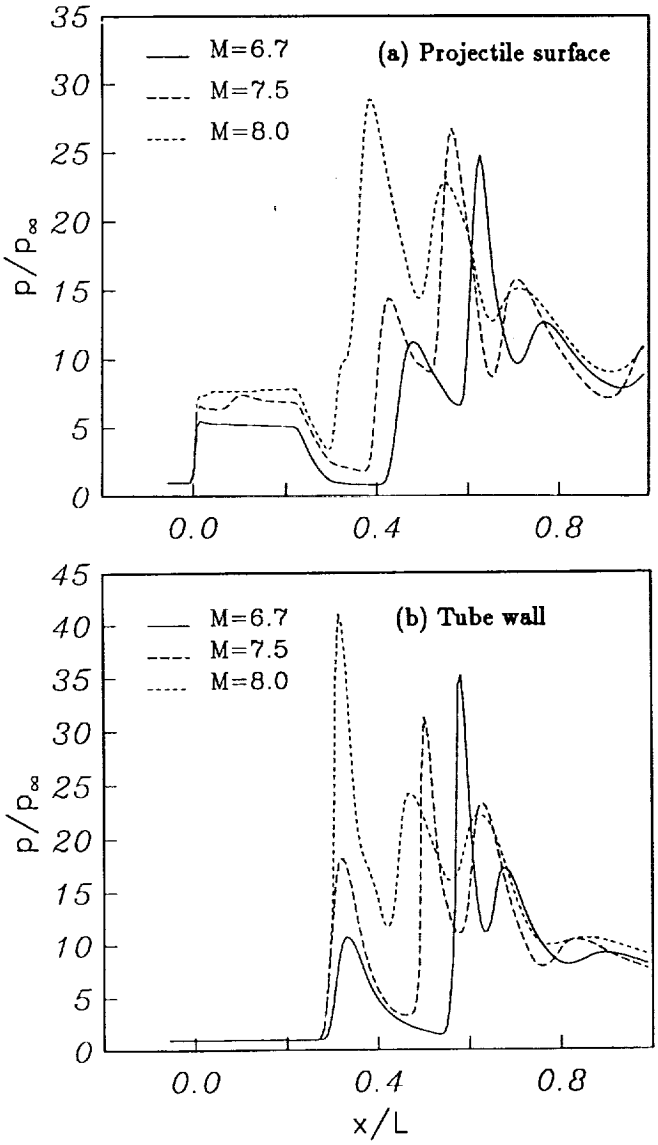

Figure. 4 Nondimensional pressure distribution along the projectile surface and tube wall for various Mach numbers.

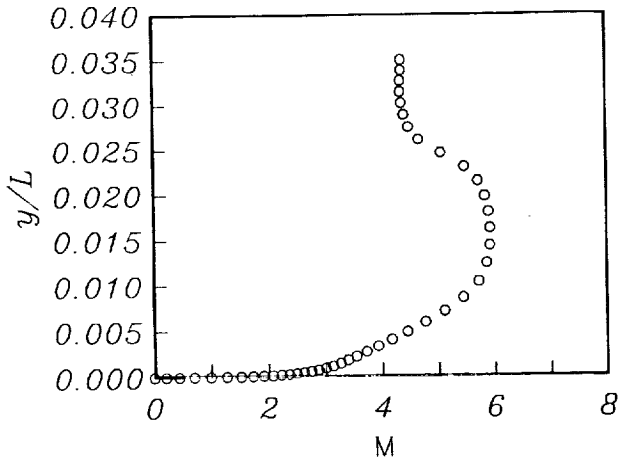

Figure. 6 Mach number as a function of vertical distance from the projectile surface, at the $x/L = 0.35$ station.

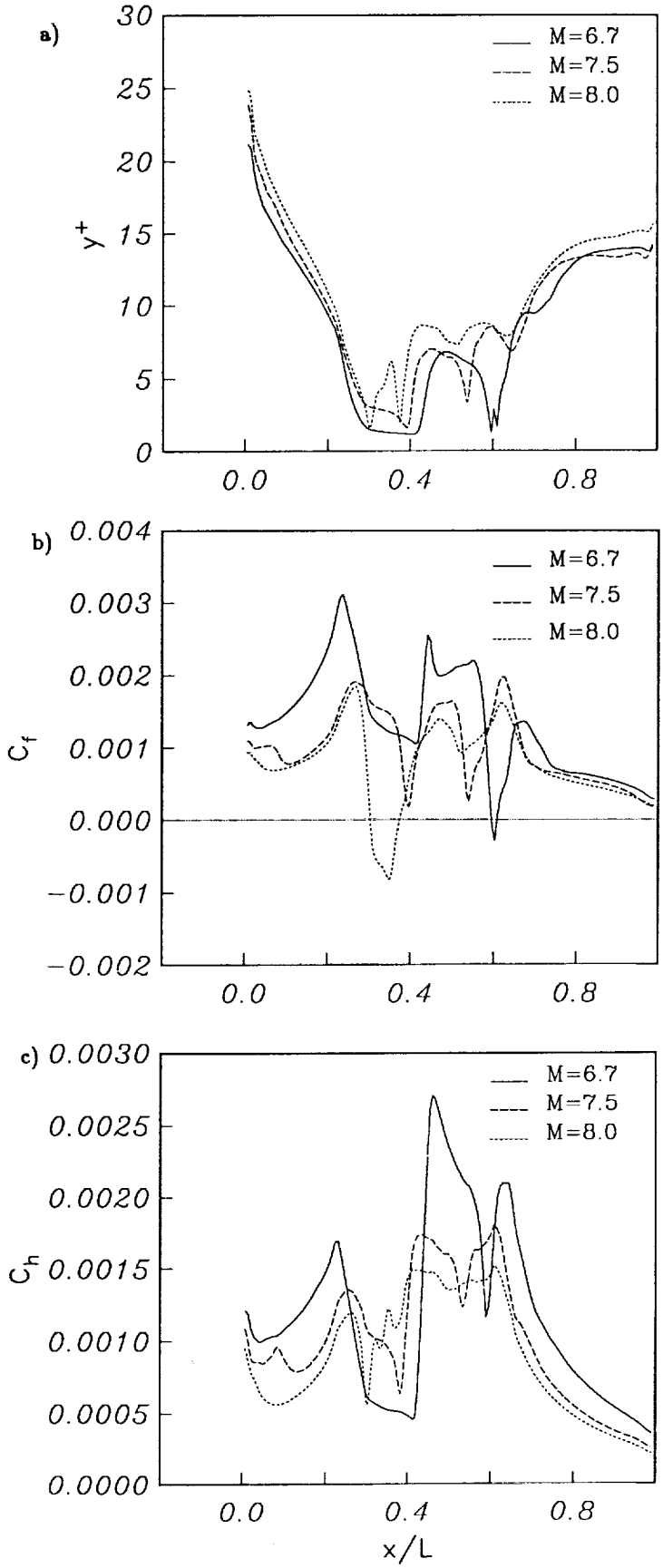

Figure. 5 Variation of y^+ (at points nearest to the wall), skin friction coefficient, and heat transfer coefficient along the projectile surface.

Figure. 7 Nondimensional temperature T/T_∞ (top half), and Mach number (bottom half) contours showing solution at several iteration stages. Mixture: $2H_2 + O_2 + 5Ar$, (turbulent flow).

ORIGINAL PAGE
COLOR PHOTOGRAPH

PRECEDING PAGE BLANK NOT FILMED

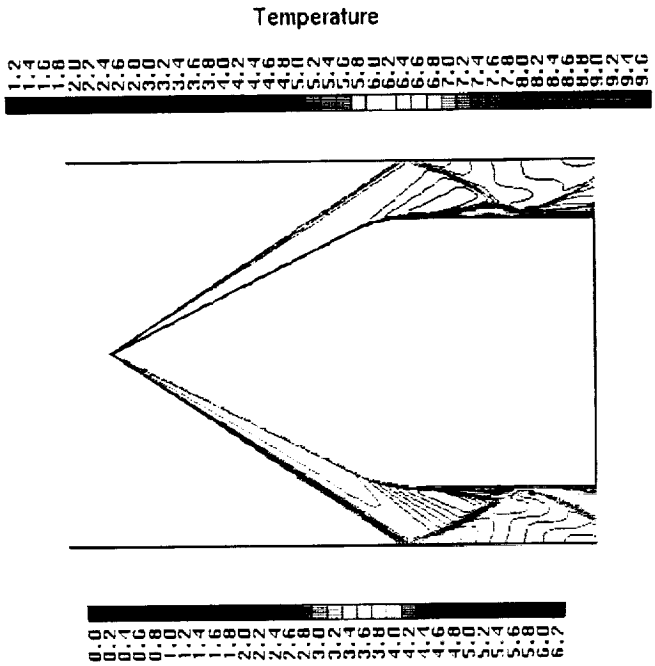

(a) Flowfield over a ram accelerator

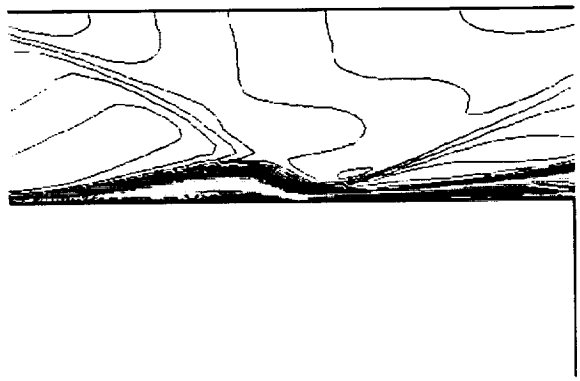

(b) Detail of shock wave/boundary layer interaction

Figure. 8 Nondimensional temperature T/T_∞, and Mach number contours showing converged solution for reacting laminar flow. Mixture: stoichiometric H_2-air, ($p_\infty = 1$ atm).

ORIGINAL PAGE
COLOR PHOTOGRAPH

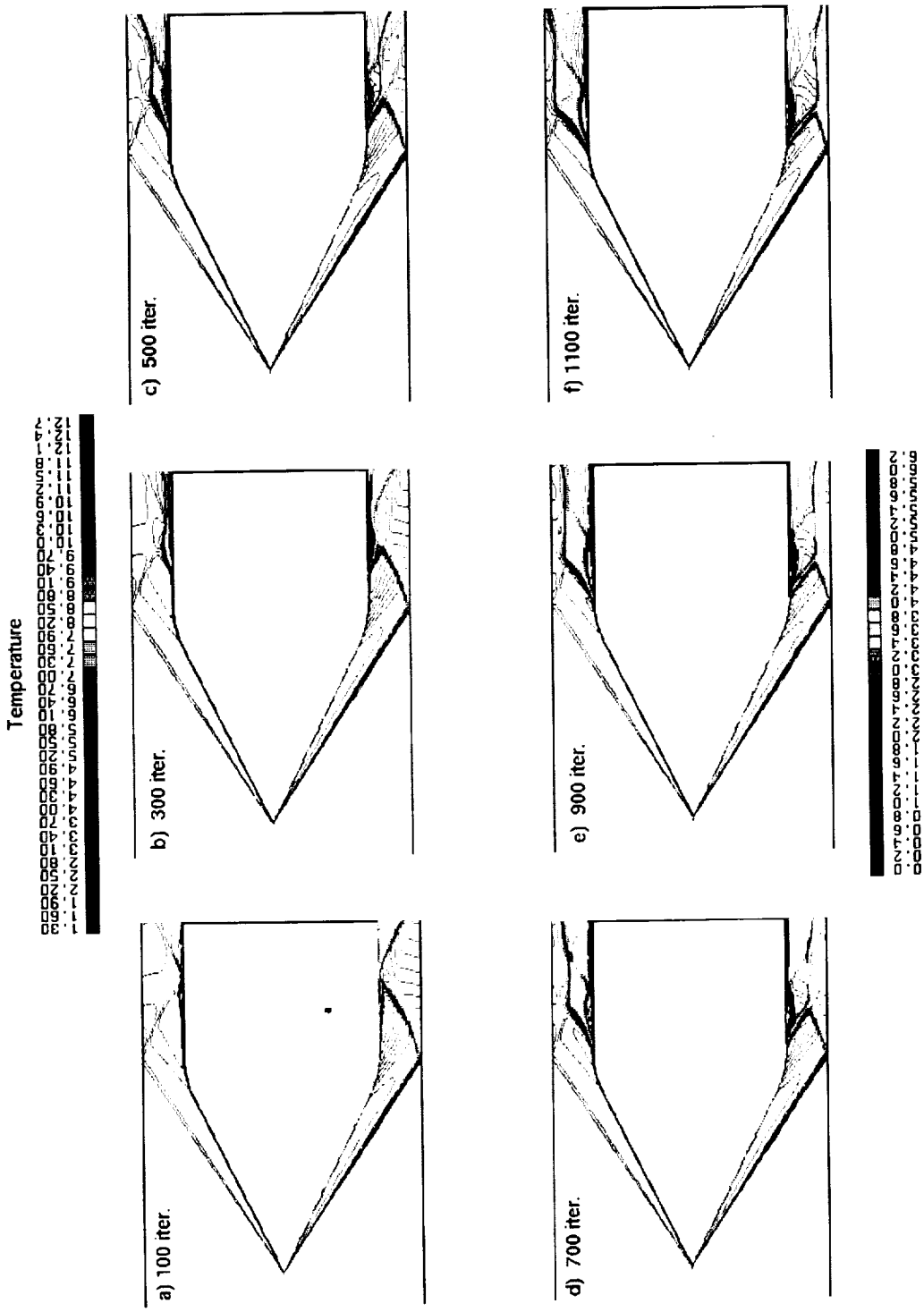

Figure. 9 Nondimensional temperature T/T_∞, and Mach number contours showing laminar flow solution at several iteration stages. Mixture: stoichiometric H_2-air, ($p_\infty = 10$ atm).

ORIGINAL PAGE
COLOR PHOTOGRAPH

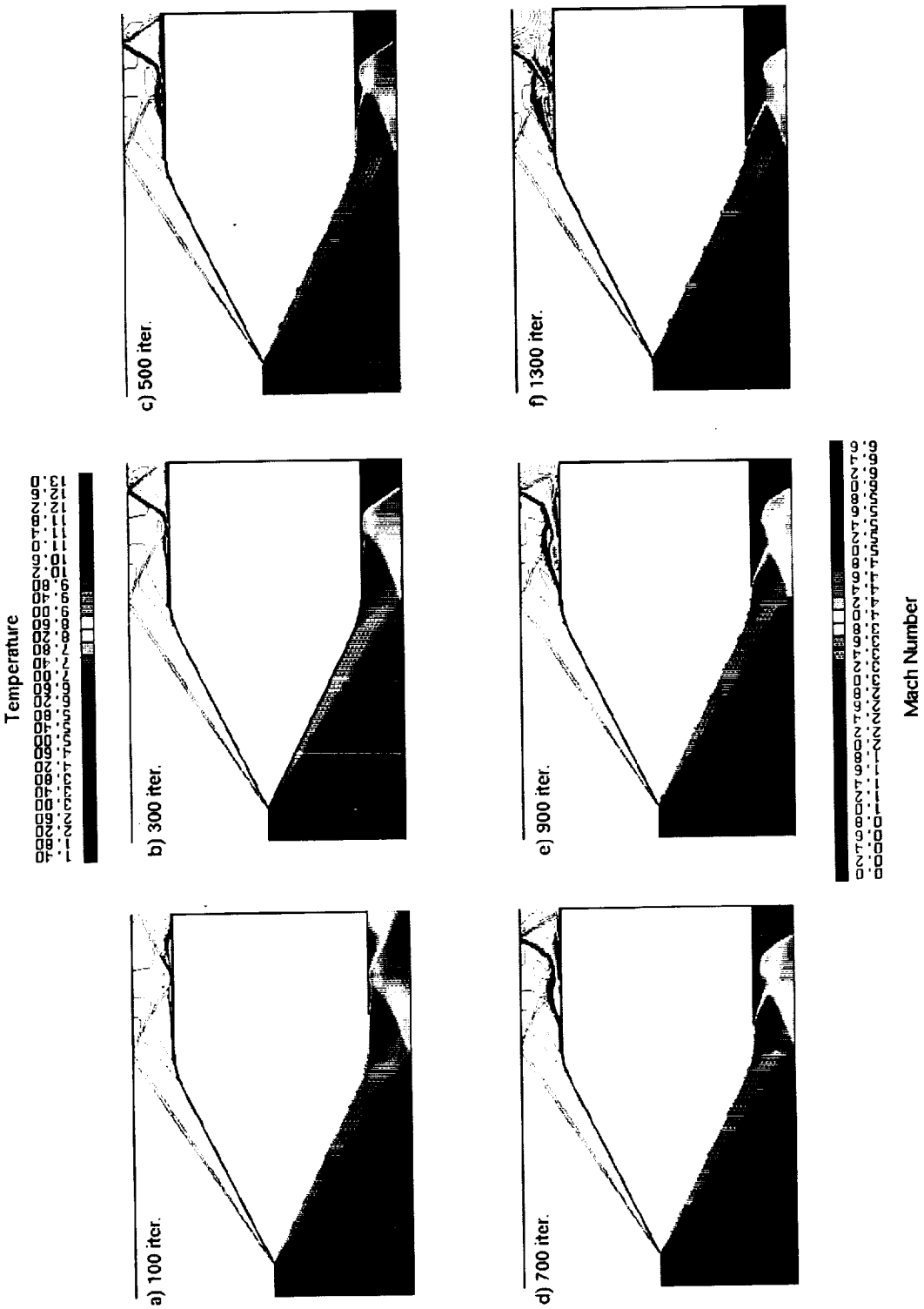

Figure. 10 Nondimensional temperature T/T_∞, and Mach number contours showing laminar flow solution at several iteration stages. Mixture: $2H_2+O_2+5Ar$, ($p_\infty = 1$ atm).

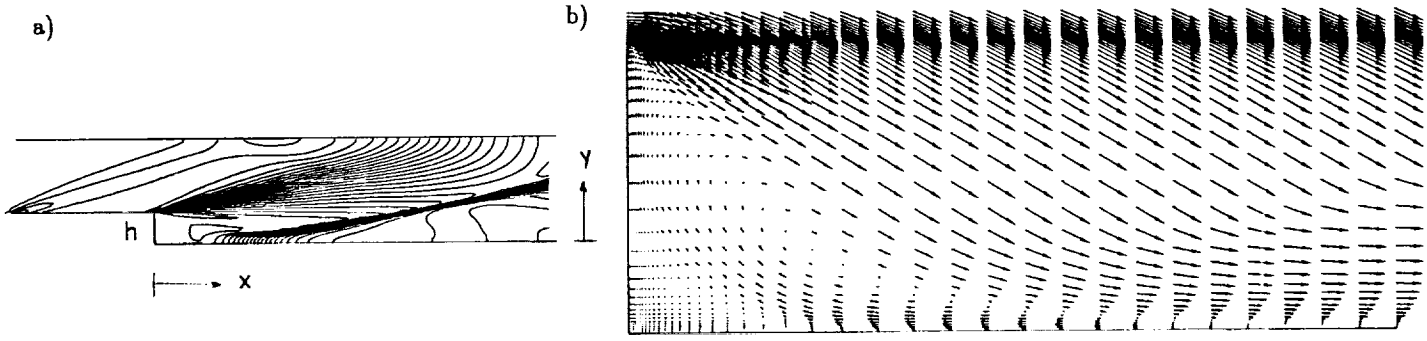

Figure 11 Pressure contours and velocity vector plot for the laminar flow over a backward facing step.

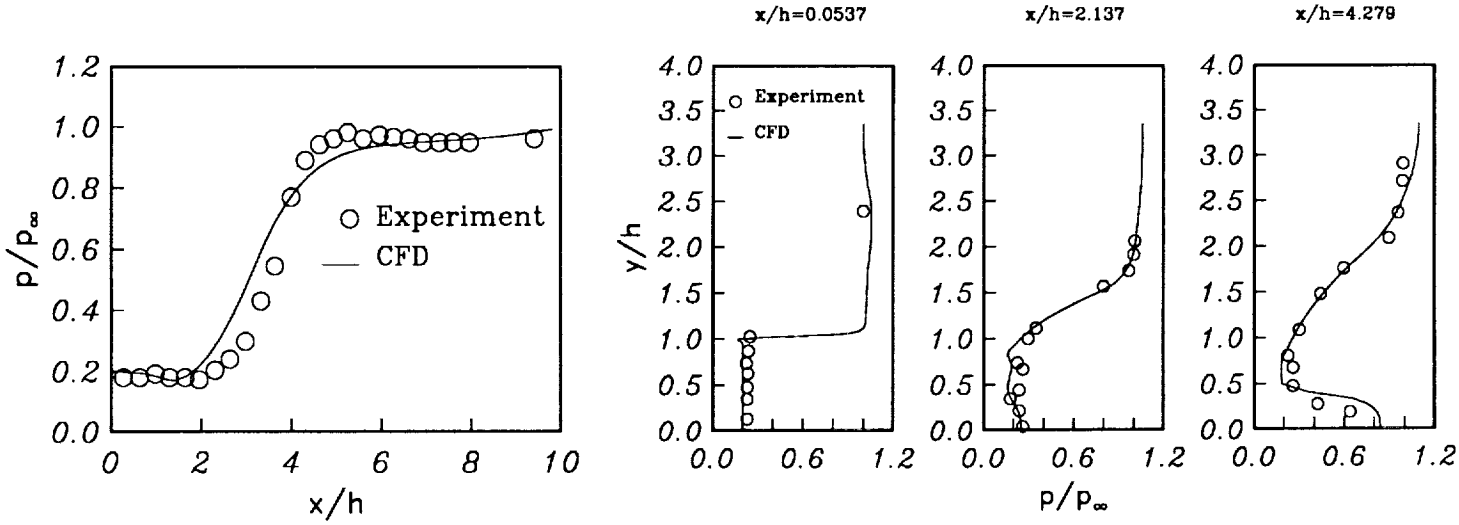

(a) Normalized wall pressure distribution

(b) Normalized pressure profiles

Figure 12 Comparison of CFD and experimental pressure distribution for laminar flow over a backward facing step.

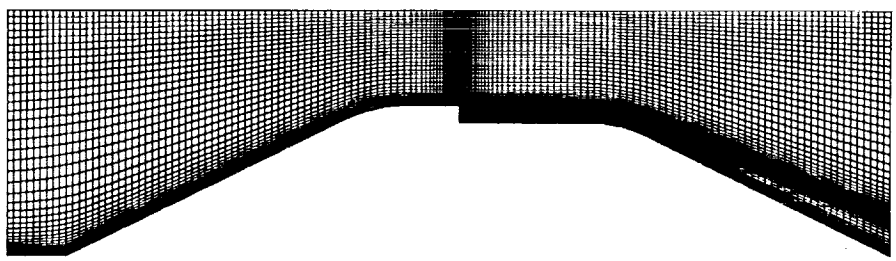

Figure 13 Computational grid.

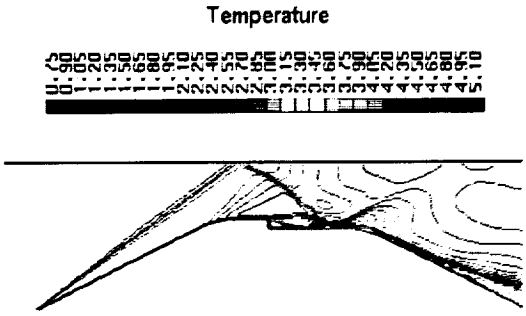

(a) Nondimensional temperature contours

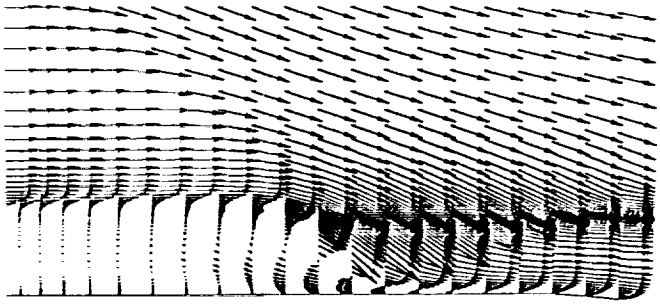

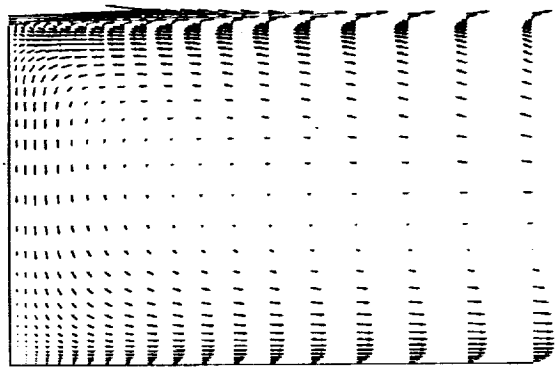

(b) Velocity vector plot behind backward facing step

Figure 14 Nonreacting converged solution for laminar flow over a ram accelerator. Mixture: $2H_2 + O_2 + 5Ar$, ($p_\infty = 1$ atm).

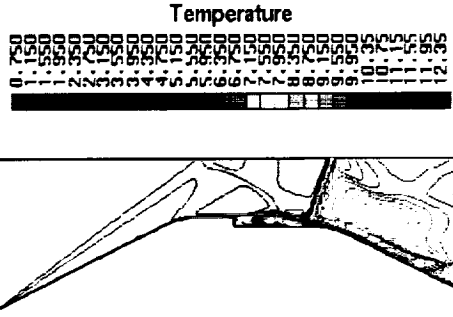

a) 100 iter.

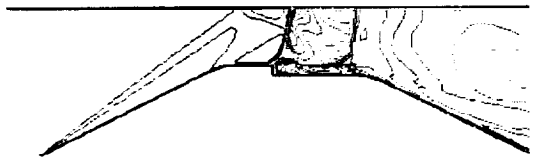

b) 200 iter.

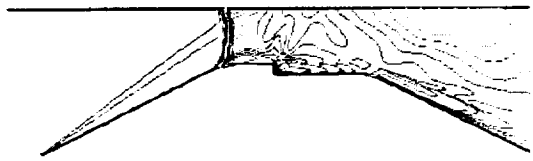

c) 600 iter.

Figure 15 Nondimensional temperature T/T_∞ contours showing reacting flow solution at several iteration stages. Mixture: $2H_2 + O_2 + 5Ar$, ($p_\infty = 1$ atm).

NASA
National Aeronautics and Space Administration

Report Documentation Page

1. Report No.	2. Government Accession No.	3. Recipient's Catalog No.
NASA TM-104439 ICOMP-91-10; AIAA-91-1916		

4. Title and Subtitle
Navier-Stokes Simulation of the Supersonic Combustion Flowfield in a Ram Accelerator

5. Report Date

6. Performing Organization Code

7. Author(s)
Shaye Yungster

8. Performing Organization Report No.
E-6278

10. Work Unit No.
505-62-21

9. Performing Organization Name and Address
National Aeronautics and Space Administration
Lewis Research Center
Cleveland, Ohio 44135-3191

11. Contract or Grant No.

13. Type of Report and Period Covered
Technical Memorandum

12. Sponsoring Agency Name and Address
National Aeronautics and Space Administration
Washington, D.C. 20546-0001

14. Sponsoring Agency Code

15. Supplementary Notes
Prepared for the 27th Joint Propulsion Conference cosponsored by the AIAA, SAE, ASME, and ASEE, Sacramento, California, June 24-27, 1991. Shaye Yungster, Institute for Computational Mechanics in Propulsion, NASA Lewis Research Center (work funded under Space Act Agreement C-99066-G). Space Act Monitor: Louis A. Povinelli, (216) 433-5818.

16. Abstract
A computational study of the ram accelerator, a ramjet-in-tube device for accelerating projectiles to ultra-high velocities, is presented. The analysis is carried out using a fully implicit TVD scheme that efficiently solves the Reynolds-averaged Navier-Stokes equations and the species continuity equations associated with a finite rate combustion model. Previous analyses of this concept have been based on inviscid assumptions. The present results indicate that viscous effects are of primary importance; in all the cases studied, shock-induced combustion always started in the boundary layer. The effects of Mach number, mixture composition, pressure, and turbulence are investigated for various configurations. Two types of combustion processes, one stable and the other unstable, have been observed depending on the inflow conditions. In the unstable case, a detonation wave is formed, which propagates upstream and unstarts the ram accelerator. In the stable case, a solution that converges to steady-state is obtained, in which the combustion wave remains stationary with respect to the ram accelerator projectile. The possibility of stabilizing the detonation wave by means of a backward facing step is also investigated. In addition to these studies, two numerical techniques have been tested. These two techniques are vector extrapolation to accelerate convergence, and a diagonal formulation that eliminates the expense of inverting large block matrices that arise in chemically reacting flows.

17. Key Words (Suggested by Author(s))	18. Distribution Statement
Hypervelocity projectiles Hypersonic combustion Detonation wave Nenequilibrium flow	Unclassified - Unlimited Subject Category 34

19. Security Classif. (of the report)	20. Security Classif. (of this page)	21. No. of pages	22. Price*
Unclassified	Unclassified	26	A03

NASA FORM 1626 OCT 86

*For sale by the National Technical Information Service, Springfield, Virginia 22161